Statistical Rate Theory Calculations of the $Cl^- + CH_3Br \rightarrow ClCH_3 + Br^-$ Rate Constant versus Temperature, Translational Energy, and H(D) Isotopic Substitution

Haobin Wang and William L. Hase*

Contribution from the Department of Chemistry, Wayne State University, Detroit, Michigan 48202

Received May 1, 1995[⊗]

Abstract: In the work presented here three different statistical theoretical models and three different potential energy surfaces are used to calculate the rate constant for the $Cl^- + CH_3Br \rightarrow ClCH_3 + Br^-$ S_N2 nucleophilic substitution reaction versus temperature, relative translational energy and CH_3Br temperature, and H(D) isotopic substitution. The calculated rate constants are compared with experimental measurements. In applying one of the theoretical models along with one of the potential energy surfaces, the potential energy for the reaction's central barrier was chosen by fitting the 300 K $Cl^- + CH_3Br$ experimental rate constant. Overall, there is poor agreement between the calculated and experimental results. The calculated temperature dependence of the $Cl^- + CH_3Br$ S_N2 rate constant is in qualitative agreement with experiment, but not quantitative. Using anharmonic vibrational frequencies, instead of harmonic, has only a small effect on the rate constant's calculated temperature dependence. The temperature dependence of the k_H/k_D isotope effect is fit by one of the theoretical models, microcanonical transition state theory, when using harmonic vibrational frequencies. However, this agreement is dramatically diminished if anharmonic vibrational frequencies are used. Differences between the calculated rate constant versus relative translational energy and CH_3Br temperature, i.e., $k(E_{rel},T)$, and experiment are striking. The decrease in the calculated $k(E_{rel},T)$, as E_{rel} is increased, is much less pronounced than observed in the experiments. Also, the calculated $k(E_{rel},T)$ increases as T is increased, while the experimental $k(E_{rel},T)$ is nearly independent of T. The inability of statistical theories to interpret the kinetics of the $Cl^- + CH_3Br$ S_N2 reaction is in accord with previous theoretical and experimental studies, which indicate the reaction's dynamics and kinetics is non-statistical.

I. Introduction

Recent experimental and theoretical studies have questioned the validity of statistical theories for gas-phase S_N2 reactions of the type[1-14]

$$X^- + CH_3Y \rightarrow XCH_3 + Y^- \quad (1)$$

In a quantum-dynamical and reaction path Hamiltonian study of the S_N2 reactions $X^- + CH_3F \rightarrow XCH_3 + F^-$ (X = H, F, OH), Basilevsky and Ryaboy[3-5] found evidence that the reactions are direct without trapping in the prereaction complex, and that the low efficiency for S_N2 reactions with a central barrier lower than the reactants' potential is due to a high probability of reflecting incoming trajectories back to reactants. In a series of papers,[6-11,13,14] classical trajectory calculations have been used to study the dynamics of the S_N2 reaction $Cl^- + CH_3Cl$ and to compare with the predictions of statistical theories. Unimolecular rate constants for $Cl^-\cdots CH_3Cl$ complexes formed by $Cl^- + CH_3Cl$ association do not agree with RRKM theory with all vibrational modes active (i.e., energy is randomly distributed among all the vibrational modes), but instead are consistent with a model in which energy is redistributed between the complex's three intermolecular modes.[14] The nine CH_3Cl intramolecular modes are only weakly coupled to the three intermolecular modes. Trajectories initialized at the central barrier remain trapped in the vicinity of the barrier with frequent barrier recrossings, a result reflective of a bottleneck for energy transfer between the complex's intermolecular and intramolecular modes.[12] Direct S_N2 nucleophilic substitution, without trapping in the $Cl^-\cdots CH_3Cl$ prereaction complex, is promoted by exciting the reactant C–Cl stretch mode, a result also consistent with weak coupling between the complex's intermolecular and intramolecular modes.[11]

Comparison between experimental measurements and predictions of statistical theories have been made for the S_N2 reaction

$$Cl^- + CH_3Br \rightarrow ClCH_3 + Br^- \quad (2)$$

Graul and Bowers[1] formed the prereaction complex $Cl^-\cdots CH_3Br$ with sufficient internal excitation to unimolecularly dissociate to products. They observed a product translational energy distribution considerably less than the prediction of statistical phase space theory. Drawing from microscopic reversibility and the previous theoretical work on $Cl^- + CH_3Cl \rightarrow ClCH_3 + Cl^-$,[6-11] they suggested that internal energy was

[⊗] Abstract published in *Advance ACS Abstracts*, August 15, 1995.

(1) (a) Graul, S. T.; Bowers, M. T. *J. Am. Chem. Soc.* **1991**, *113*, 9696. (b) Graul, S. T.; Bowers, M. T. *J. Am. Chem. Soc.* **1994**, *116*, 3875.
(2) Viggiano, A. A.; Morris, R. A.; Paschkewitz, J. S.; Paulson, J. F. *J. Am. Chem. Soc.* **1992**, *114*, 10477.
(3) Basilevsky, M. V.; Ryaboy, V. M. *Chem. Phys. Lett.* **1986**, *129*, 71.
(4) Ryaboy, V. M. *Chem. Phys. Lett.* **1989**, *159*, 371.
(5) Ryaboy, V. M. In *Advances in Classical Trajectory Methods*, Vol. 2, *Dynamics of Ion–Molecule Complexes*: Hase, W. L., Ed.; JAI Press: Greenwich, CT, 1993.
(6) Vande Linde, S. R.; Hase, W. L. *J. Am. Chem. Soc.* **1989**, *111*, 2349.
(7) Vande Linde, S. R.; Hase, W. L. *J. Phys. Chem.* **1990**, *94*, 2778.
(8) Vande Linde, S. R.; Hase, W. L. *J. Phys. Chem.* **1990**, *94*, 6148.
(9) Vande Linde, S. R.; Hase, W. L. *J. Chem. Phys.* **1990**, *93*, 7962.
(10) Cho, Y. J.; Vande Linde, S. R.; Zhu, L.; Hase, W. L. *J. Chem. Phys.* **1992**, *96*, 8275.
(11) Hase, W. L.; Cho, Y. J. *J. Chem. Phys.* **1993**, *98*, 8626.
(12) Wang, H.; Peslherbe, G. H.; Hase, W. L.; *J. Am. Chem. Soc.* **1994**, *116*, 9644.
(13) Hase, W. L. *Science* **1994**, *266*, 998.
(14) Peslherbe, G. H.; Wang, H.; Hase, W. L. *J. Chem. Phys.* **1995**, *102*, 5626.

0002-7863/95/1517-9347$09.00/0

not randomized among all vibrational modes as predicted by statistical theory, and, instead, the C−Cl stretch and/or CH_3 umbrella modes of the CH_3Cl product may be preferentially excited. Viggiano and co-workers[2] measured the rate constants of reaction 2 versus reagent relative translational energy and CH_3Br temperature. For a fixed relative translational energy, they found the rate constant does not depend on the temperature of CH_3Br and, thus, the CH_3Br vibrational/rotational energy. At first glance, this result seems inconsistent with Rice-Ramsperger-Kassel-Marcus (RRKM) theory, which predicts that the ratio of the rate constants for Cl^-- - -CH_3Br decomposition to $Cl^- + CH_3Br$ and $ClCH_3 + Br^-$ varies with CH_3Br internal energy.[15] However, this experimental result has been reproduced by a calculation combining average dipole orientation (ADO) and RRKM theories.[1b] An important experimental measurement is the pressure dependence of the rate constant for reaction 2,[16] since it may reveal the lifetime of the Cl^-- - -CH_3Br complex, which can be compared with that of RRKM theory. The rate constant increases with an increase in pressure,[16] and the test of transition state theory may be most complete at high pressure where there is a Boltzmann distribution of energy states at the $[Cl$- - -CH_3- - -$Br]^-$ central barrier.

Trajectory calculations have been performed to assist in interpreting the experimental studies of reaction 2.[12] These calculations showed that, as for the Cl^-- - -CH_3Cl complex,[10,11] the decomposition of the Cl^-- - -CH_3Br complex is mediated by two distinct types of modes. The intermolecular modes are coupled to the dissociation channel forming $Cl^- + CH_3Br$, while the intramolecular modes have access to the central barrier. The trajectory $ClCH_3 + Br^-$ product energy distribution is different from that calculated by phase space theory, but consistent with the measurement of Graul and Bowers.[1]

Despite the above examples of the possible incompleteness of statistical models, statistical theories such as transition state theory, RRKM theory, and phase space theory remain valuable tools in predicting and interpreting S_N2 kinetics and dynamics. For example, Truhlar and co-workers[17] used transition state theory and a parametrized AM1 reaction path calculation to qualitatively explain the kinetic isotope effect of reaction 2. Brauman and co-workers[18] successfully used microcanonical variational transition state theory (μCVTST) to explain the kinetics of the $ClCH_2CN + Cl^- \rightarrow Cl^- + ClCH_2CN$ reaction. Su and co-workers[19] used a trajectory capture model, similar to μCVTST, to study $X^- + CH_3Y$ association to form the X^-- - -CH_3Y complex. These studies have given either qualitative or quantitative agreement with the experimental results.

In this paper, different statistical models are used to calculate the rate constant for reaction 2. Reaction path information based on an analytical potential energy function and different levels of *ab initio* theory are used in the calculations. To account for anharmonic effects, frequencies along the reaction path are scaled by factors determined by comparing experimental anharmonic and *ab initio* frequencies for CH_3Br and CH_3Cl. The calculated rate constants and kinetic isotope effects are compared with both experimental results and the previous theoretical calculations. These comparisons provide further insight into the dynamics of S_N2 reactions.

Table 1. Energies and Structures[a]

property	expt[b]	PES1(Br)[c]	HF[c,d]	MP2[c,d]
		Reactant, CH3Br		
R_{C-Br}	1.934	1.944	1.944	1.939
R_{H-C}	1.082	1.077	1.076	1.087
θ_{H-C-Br}	10.77	107.6	107.8	107.8
energy	0	0	0	0
		Complex, Cl^-- - -CH_3Br		
R_{Cl-C}		3.221	3.216	3.076
R_{Cl-Br}		1.991	1.997	1.994
R_{H-C}		1.071	1.071	1.083
θ_{H-C-Br}		107.1	106.8	107.1
energy	-10 ± 1[e]	−10.73	−10.74	−12.59
		Central Barrier		
R_{Cl-C}		2.470	2.469	2.394
R_{Cl-Br}		2.462	2.458	2.405
R_{H-C}		1.062	1.062	1.074
θ_{H-C-Br}		92.6	92.2	92.2
energy		−2.79	−2.91	−5.21

[a] Distances are in angstroms, angles are in degrees, and energies in kcal/mol. [b] The experimental relative energies are for 0 K and include zero-point energies. The CH_3Br experimental geometry is taken from ref 22. [c] The PES1(Br), HF, and MP2 relative energies are electronic energies and do not include zero-point energies. [d] The HF and MP2 ab initio calculations were performerd with the SV4PP/6-31G* basis set. [e] Taken from ref 23.

The outline of the remaining part of the paper is as follows. In Section II the different potential energy surfaces used in the calculations are described. The different statistical models used to calculate the rate constant for reaction 2 as a function of temperature, center-of-mass relative translational energy, and CH_3Br internal temperature are described in Section III. The results of the calculations are presented in Section IV. Section V is the summary.

II. Potential Energy Surfaces

Three different potential energy surfaces were used for the calculations reported here. Two are *ab initio* surfaces determined at the HF and MP2 levels of theory, with a split valence contracted Gaussian basis, i.e., the SV4PP basis set developed by Andzelm et al.[20] for Cl and Br and the 6−31G* basis set for CH_3. These two basis sets have similar sizes and are, thus, considered compatible. Both the HF (reported previously[15]) and MP2 calculations were performed with the Gaussian 92 series of programs.[21] The third surface is the analytic potential energy function PES1(Br), fit to the HF/SV4PP/6-31G* calculations and described in ref 15.

The structures and energies, given by the above three potential energy surfaces for CH_3Br, the Cl^-- - -CH_3Br complex, and the $[Cl$- - -CH_3- - -$Br]^-$ central barrier, are listed in Table 1, where they are compared with experimental values.[22,23] Harmonic and anharmonic frequencies for these three structures are listed in Table 2. In previous work,[22] experimental harmonic frequencies for CH_3Br (CD_3Br) were determined from the measured anharmonic frequencies by employing Dennison's rule, i.e.

(15) Wang, H.; Zhu, L.; Hase, W. L. *J. Phys. Chem.* **1994**, *98*, 1608.
(16) (a) Giles, K.; Grimsrud, E. P. *J. Phys. Chem.* **1992**, *96*, 6680. (b) Knighton, W. B.; Bognar, J. A.; O'Connor, P. M.; Grimsrud, E. P. *J. Am. Chem. Soc.* **1993**, *115*, 12079.
(17) Viggiano, A. A.; Paschkewitz, J. S.; Morris, R. A.; Paulson, J. F.; Gonzalez-Lafont, A.; Truhlar, D. G. *J. Am. Chem. Soc.* **1991**, *113*, 9404.
(18) Wladkowski, B. D.; Lim, K. F.; Allen, W. D.; Brauman, J. I. *J. Am. Chem. Soc.* **1992**, *114*, 9136.
(19) 9 (a) Su, T.; Chesnavich, W. J. *J. Chem. Phys.* **1982**, *76*, 5183. (b) Su, T. *J. Chem. Phys.* **1985**, *82*, 2164.
(20) Andzelm, J.; Klobukowski, M.; Radzio-Andzelm, E. *J. Comput. Chem.* **1984**, *5*, 146.
(21) Frisch, J. M.; Trucks, G. W.; Head-Gordon, M.; Gill, P. M. W.; Wong, M. W.; Foresman, J. B.; Johnson, B. G.; Schlegel, H. B.; Robb, M. A.; Replogle, E. S.; Gomperts, R.; Andrés, J. L.; Raghavachari, K.; Binkley, J. S.; Gonzalez, C.; Martin, R. L.; Fox, D. J.; DeFrees, D. J.; Baker, J.; Stewart, J. J. P.; Pople, J. A.; *GAUSSIAN 92*, Gaussian, Inc.: Pittsburgh, PA, 1992.
(22) Duncan, J. L.; Allan, A.; McKean, D. C. *Mol. Phys.* **1970**, 18, 289.
(23) Caldwell, G.; Magnera, T. F.; Kebarle, P. *J. Am. Chem. Soc.* **1984**, *106*, 959.

Table 2. Harmonic and Anharmonic Frequencies[a]

mode	expt	PES1(Br)[b]	HF[c]	MP2[d]
		CH_3Br		
A_1, C−Br str	617 (611)	620 (611)	642 (573)	627 (591)
	582 (576)	552 (576)	605 (540)	590 (556)
E, CH_3 rock	974 (955)	1065 (955)	1066 (952)	1015 (957)
	724 (713)	796 (713)	792 (707)	755 (712)
A_1, CH_3 deform	1333 (1306)	1497 (1306)	1484 (1325)	1401 (1321)
	1007 (992)	1190 (992)	1121 (1001)	1058 (997)
E, CH_3 deform	1472 (1443)	1457 (1443)	1620 (1446)	1537 (1449)
	1071 (1055)	1047 (1055)	1175 (1049)	1115 (1051)
A_1, C−H str	3082 (2959)	3048 (2959)	3278 (2927)	3160 (2979)
	2211 (2147)	2189 (2147)	2342 (2091)	2259 (2130)
E, C−H str	3184 (3057)	3183 (3057)	3392 (3029)	3283 (3095)
	2368 (2299)	2373 (2299)	2521 (2251)	2440 (2300)
		Complex, Cl^-- - -CH_3Br		
E, Cl^- bend		72 (71)	71 (63)	80 (75)
		65 (64)	64 (57)	71 (67)
A_1, Cl−C str		91 (90))	94 (84)	108 (102)
		89 (88)	93 (83)	108 (102)
A_1, C−Br str		500 (493)	518 (463)	518 (488)
		464 (484)	497 (444)	497 (469)
E, CH_3 rock		1089 (977)	1032 (921)	972 (916)
		812 (727)	764 (682)	720 (679)
A_1, CH_3 deform		1467 (1280)	1420 (1268)	1322 (1246)
		1128 (940)	1054 (941)	982 (926)
E, CH_3 deform		1452 (1438)	1595 (1424)	1509 (1423)
		1042 (1050)	1159 (1035)	1097 (1034)
A_1, C−H str		3147 (3055)	3334 (2977)	3207 (3023)
		2252 (2209)	2379 (2124)	2289 (2158)
E, C-H str		3293 (3163))	3471 (3099)	3349 (3157)
		2455 (2378)	2582 (2305)	2489 (2346)
		Central Barrier		
E, Cl−C−Br bend		169 (167)	183 (163)	187 (176)
		156 (154)	169 (151)	178 (168)
A_1, Cl−C−Br str		161 (159)	172 (154)	193 (182)
		158 (156)	172 (154)	186 (175)
E, CH_3 rock		1155 (1036)	974 (870)	973 (917)
		814 (729)	691 (617)	690 (650)
A_2, out-of-plane bend		1185 (1034)	1203 (1074)	1069 (1008)
		847 (706)	867 (774)	767 (723)
E, CH_3 deform		1340 (1327)	1549 (1383)	1459 (1375)
		982 (990)	1139 (1017)	1074 (1012)
A_1, C−H str		3215 (3121)	3418 (3052)	3267 (3080)
		2274 (2230)	2418 (2159)	2311 (2179)
E, C-H str		3415 (3280)	3630 (3241)	3475 (3276)
		2554 (2474)	2711 (2420)	2594 (2445)
reaction coordinate		400 i	380 i	427 i
		400 i	378 i	427 i

[a] The frequencies are given in units of cm^{-1}. The frequencies in parentheses are the anharmonic values. The frequencies in the second row, for each frequency type, are for the CD_3Br isotope. [b] Anharmonic frequencies for the PES1(Br) surface were determined by scaling the harmonic PES1(Br) CH_3Br frequencies to the experimental anharmonic ones. Individual scale factors were determined for each of the CH_3Br modes in the Cl^-- - -CH_3Br complex, central barrier, and $Cl^- + CH_3Br \rightarrow Cl^-$- - -$CH_3Br$ reaction path. Cl−C−Br corresponding modes are not present in CH_3Br for the Cl−C stretch and Cl−C−Br bending modes. Thus, the 0.99 and 0.98 scale factors, for the Cl−C stretch in CH_3Cl and CH_3 deformation in CH_3Br, respectively, were used to scale the harmonic frequencies for these two modes. [c] The anharmonic frequencies for the HF/SV4PP/6−31G* surface were determined by multiplying the harmonic frequencies by the factor 0.8929; ref 24a. [d] The anharmonic frequencies for the MP2/SV4PP/6−31G* surface were determined by multiplying the harmonic frequencies by the factor 0.9427; ref 24b.

$$\nu_H = \omega_H(1 - x_H) \tag{3a}$$

$$x_D = x_H(\nu_D/\nu_H) \tag{3b}$$

where ν and ω represent the anharmonic and harmonic frequencies, respectively, and ν_H and ν_D refer to the same mode in CH_3Br and CD_3Br. The values of x are 0.04 for CH stretching, 0.02 for CH bending, and 0.01 for C−Br stretching.

Harmonic frequencies for PES1(Br) and the HF and MP2 *ab initio* surfaces were determined by a standard normal mode analysis. Anharmonic frequencies for PES1(Br) were determined by scaling the PES1(Br) harmonic frequencies to match the experimental anharmonic ones. This yielded individual scale factors for each of the CH_3Br modes, which were used to scale the harmonic frequencies for the corresponding modes in the Cl^-- - -CH_3Br complex, central barrier, and $Cl^- + CH_3Br \rightarrow Cl^-$- - -$CH_3Br$ reaction path. Corresponding modes are not present in CH_3Br for the Cl−C stretch and Cl−C−Br bending modes. The experimental anharmonic/harmonic frequency ratio for the Cl−C stretch in CH_3Cl, 0.99, is used to scale the harmonic frequencies for the Cl−C stretch. The CH_3 deformation and rock frequencies of CH_3Br have the same experimental anharmonic/harmonic frequency ratio of 0.98, which is used to scale the harmonic frequencies for the Cl−C−Br bend. Anharmonic frequencies for the HF and MP2 surfaces were determined by scaling the harmonic frequencies by the widely used scale factors of 0.8929[24a] and 0.9427,[24b] respectively.

(24) (a) Pople, J. A.; Head-Gordon, M.; Fox, D. J.; Raghavachari, K.; Curtiss, L. A. *J. Chem. Phys.* **1989**, *90*, 5622. (b) Pople, J. A.; Scott, A. P.; Wong, M. W.; Radom, L. *Isr. J. Chem.* **1993**, *33*, 345.

The classical potential energy difference between the central barrier and the reactants is −2.91, −5.21, and −2.79 kcal/mol for the HF, MP2, and PES1(Br) surfaces, respectively. With zero-point energy added using the harmonic frequencies, the respective potential energy differences are −3.05, −5.41, and −2.58 kcal/mol. These potential energy differences become −3.03, −5.40, and −2.58 kcal/mol if the anharmonic frequencies are used.

III. Statistical Models for the S_N2 Rate Constant

A. S_N2 Rate Constant Versus E_{rel} and CH_3Br Temperature. To use statistical theories to calculate the rate of reaction 2 as a function of the CH_3Br temperature T and $Cl^- + CH_3Br$ relative translation energy E_{rel}, the following mechanism is assumed:

$$Cl^- + CH_3Br \underset{k_{dis}}{\overset{k_{cap}}{\rightleftharpoons}} Cl^- \cdots CH_3Br \xrightarrow{k_{isom}} ClCH_3 + Br \quad (4)$$

Steps for the formation and the decomposition of the $ClCH_3 \cdots Br^-$ complex are not included in the mechanism, since the mechanism is based on statistical assumptions and RRKM calculations[12] show that this complex preferentially dissociates to $ClCH_3 + Br^-$. Su[25] has parametrized the results of trajectory calculations for ion−molecule collisions to determine k_{cap} in eq 4 versus E_{rel} and T. The interaction potential used in the trajectory capture calculations is the ion-dipole/ion-induced-dipole potential

$$V = -\frac{\alpha q^2}{2r^4} - \frac{q\mu_D}{r^2}\cos\theta \quad (5)$$

where α and μ_D are the polarizability and dipole moment for the neutral molecule, r is the distance between the ion and the center of mass of the neutral molecule, θ is the angle formed by the dipole and r, and q is the charge of the ion. The capture rate constant is given by[25]

$$k_{cap}(E_{rel},T) = K_c(\tau,\epsilon)k_L \quad (6)$$

where k_L is the Langevin rate constant[26] and $K_c(\tau,\epsilon)$ is the parametrized "locking constant"[25] which depends on

$$\tau = \frac{\mu_D}{\sqrt{\alpha T}} \quad (7)$$

and

$$\epsilon = \frac{\mu_D}{\sqrt{\alpha E_{rel}}} \quad (8)$$

According to the above assumption, once the $Cl^- \cdots CH_3Br$ complex is formed, the probability of product formation is given by $k_{isom}/(k_{isom} + k_{dis})$. Thus, to obtain the S_N2 rate constant for fixed E_{rel} and T, the above $k_{cap}(E_{rel},T)$ is combined with an energy and angular momenta average of this probability to give

$$k_{S_N2}(E_{rel},T) = k_{cap}(E_{rel},T)\sum_{l=0}^{l_{max}} P(l) \times \sum_{j=0}^{\infty}\sum_{j_z=-j}^{j} P(j,j_z)\sum_{n=0}^{\infty} P(\mathbf{n})\sum_{J=|l-j|}^{J=|l+j|} P(J)\frac{k_{isom}(E,J)}{k_{dis}(E,J)+k_{isom}(E,J)} \quad (9)$$

where $P(l)$ is the normalized probability density of forming the $Cl^- \cdots CH_3Br$ complex by collisions with orbital angular momentum quantum number l. $P(l)$ is related to the collision impact parameter b by $P(l) \propto bP_r(b)$, where $P_r(b)$ is the probability of complex formation for collisions with b. For the calculation reported here no dynamical information was used to determine $P(l)$ and $P_r(b)$ was set to unity. To find the maximum impact parameter b_{max} for complexation and, thus, l_{max} for $P(l)$, the trajectory capture rate constant is written as

$$k_{cap}(E_{rel},T) = v_{rel}\sigma_{cap}(E_{rel},T) \quad (10a)$$

and the capture cross section as

$$\sigma_{cap}(E_{rel},T) = \int_0^{b_{max}} P_r(b)2\pi b\, db \quad (10b)$$

To compare with the above model for finding $P(l)$ and l_{max}, classical trajectory calculations were performed to determine b_{max} and $P_r(b)$ at various E_{rel} and T. Overall the trajectory and model $P(l)$ distributions are very similar. Their only significant difference is that the trajectory $P_r(b)$ is not square with a value of unity between 0 and b_{max} but, instead, has a rapidly diminishing tail at large b which tends to a value of b_{max} 20% larger than that for the above model. This has a minimal effect on the S_N2 rate constant. Rate constants calculated from eq 9, with the trajectory $P(l)$, are within 5% of those reported here for the above model $P(l)$.

$P(j,j_z)$ in eq 9 is the probability density of CH_3Br total rotational angular momentum quantum number j and rotational quantum number j_z. It is given by

$$P(j,j_z) = \frac{(2j+1)\exp\{(-\hbar^2/2k_BT)[j(j+1)/I_A + j_z^2(1/I_C - 1/I_A)]\}}{Q_{rot}} \quad (11)$$

where Q_{rot} is the CH_3Br rotational partition function, and I_A and I_C are the two principal moments of inertia with I_c the one for the symmetric axis. The symmetry number in the partition function is removed and merged into the reaction path degeneracy factor, which for reaction 2 is one.

$P(\mathbf{n})$ in eq 9 is the probability distribution of vibrational energy for each set of CH_3Br vibrational quantum numbers $\mathbf{n}$ at temperature T, which is given by

$$P(\mathbf{n}) = \prod_{i=1}^{9} \exp(-n_i h\nu_i/k_BT)[1 - \exp(-h\nu_i/k_BT)] \quad (12)$$

with $\mathbf{n} = \{n_1, n_2, \ldots, n_9\}$. $P(J)$ in eq 9 is the probability distribution of total angular momentum quantum number J, which is given by the combination of orbital angular momentum quantum number l and the CH_3Br rotational angular momentum quantum number j; i.e.

$$P(J) = \frac{2J+1}{(2l+1)(2j+1)} \quad (13)$$

The energy E in eq 9 can be written as:

(25) Su, T. *J. Chem. Phys.* **1994**, *100*, 4703.
(26) (a) Langevin, P. M. *Ann. Chem. Phys.* **1905**, *5*, 245. (b) Gioumousis, G.; Stevenson, D. P. *J. Chem. Phys.* **1958**, *29*, 294.

$$E = E_{rel} + \sum_{i=1}^{9} n_i h\nu_i + \frac{j(j+1)\hbar^2}{2I_A} + \frac{j_z^2\hbar^2}{2}\left[\frac{1}{I_C} - \frac{1}{I_A}\right] \quad (14)$$

The rate constants $k_{isom}(E,J)$ and $k_{dis}(E,J)$ in eq 9 are given by the RRKM expression

$$k(E,J) = \frac{N^{\ddagger}(E,J)}{h\rho(E,J)} \quad (15)$$

where $N^{\ddagger}(E,J)$ is the transition state sum of states and $\rho(E,J)$ the $Cl^-\cdots CH_3Br$ complex's density of states. Inserting the RRKM expressions for $k_{isom}(E,J)$ and $k_{dis}(E,J)$ into eq 9 gives

$$k_{S_N2}(E_{rel},T) = k_{cap}(E_{rel},T) \sum_{l=0}^{l_{max}} P(l) \sum_{j=0}^{\infty} \sum_{j_z=-j}^{j} P(j,j_z) \sum_{n=0}^{\infty} P(\mathbf{n}) \sum_{J=|l-j|}^{J=|l+j|} P(J) \frac{N^{\ddagger}_{bar}(E,J)}{N^{\ddagger}_{var}(E,J) + N^{\ddagger}_{bar}(E,J)} \quad (16)$$

where $N^{\ddagger}_{bar}(E,J)$ is the sum of states for the central barrier transition state and $N^{\ddagger}_{var}(E,J)$ is the sum of states for the $Cl^-\cdots CH_3Br \rightarrow Cl^- + CH_3Br$ microcanonical variational transition state (see next section). Equation 16 is similar to those used by Wladkowski et al.[18] and Graul and Bowers[1b] to calculate the S_N2 rate constant.

Equation 16 involves a 5-dimensional summation over the quantum numbers l, j, j_z, $\mathbf{n}$, and J. The summation over l is finite and extends to l_{max}. The upper summation limits for j and $\mathbf{n}$, which are not finite, were set at the values where $P(j,j_z)$ and $P(\mathbf{n})$ are equal to 0.001. Tests showed that choosing these limiting values gave rate constants accurate to within three significant figures. The summation limits for j_z and J are set by the limits for l and j.

Since CH_3Br has nine vibrational modes, one way to carry out the summation over $\mathbf{n}\{n_1, n_2, ..., n_9\}$ in eq 16 is to perform a 9-dimensional summation. However, even though some of the CH_3Br modes have high frequencies, for which only 2−3 quantum states contribute to the rate constant, performing a 9-dimensional summation is very uneconomical for it includes at least 2^9−3^9 terms. The approach used here was to consider all combinations of the quantum numbers n_1, n_2, ..., n_9 and only retain the combinations that gave a probability greater than 0.001. This is equivalent to changing the 9-dimensional summation to a 1-dimensional summation over a vector, which depends on nine quantum numbers. This was a very efficient approach for, at the highest temperature in our calculation, there were only 20 terms (i.e., states) in the summation.

For the summation over l, j,j_z, and J in eq 16, a direct summation was performed if the number of terms in the summation was 40 or less; otherwise 10-point Gauss−Legendre quadrature was performed. Since the summations are over integer quantum numbers, the quadrature points, which are non-integers, were truncated to the nearest integer value. Truncation was necessary to evaluate the sums of states in eq 16 versus integer J. Tests, in which the 10-point Gauss−Legendre quadratures were replaced by direct summations and 40-point Gauss−Legendre quadratures, showed that the use of 10-point quadratures in the above manner gives rate constants with three significant figure accuracy.

The most time-consuming part of the calculation was the determination of the positions and sums of states for the variational transition states. The Whitten−Rabinovitch (WR) approximation[27] was not sufficiently accurate for evaluating the sum of states (see below) and the Beyer−Swinehart (BS)[28] direct count algorithm was needed. A direct evaluation of eq 16 would require a minimum of 10^8 calls to this algorithm. This is because up to 100 sums of states are calculated along the reaction path to find an accurate minimum in the sum of states, 10-point Gauss−Legendre quadrature approximates the sum over K to determine $N^{\ddagger}_{var}(E,J)$ [see next section], and at least 10^5 calls are needed to complete the 5-dimensional summation. Such a calculation requires a prohibitive amount of computer time. To make the evaluation of eq 16 feasible, a two-dimensional grid of $N^{\ddagger}_{var}(E,J)$ was formed at intervals of 5 for J and 0.1 kcal/mol intervals for E < 10 kcal/mol and 0.5 kcal/mol intervals for $E \geq 10$ kcal/mol. Since the change in $N^{\ddagger}_{var}(E,J)$ with E and J is smooth, cubic splines could be used to interpolate the values of $N^{\ddagger}_{var}(E,J)$ needed for solving eq 16.

B. S_N2 Rate Constant versus Temperature. Three different models were used to calculate the rate constant for reaction 2 versus temperature. For one model, called the capture/RRKM model, the S_N2 rate constant in eq 16 versus E_{rel} and CH_3Br temperature T is averaged over the Boltzmann distribution for E_{rel} at temperature T to obtain $k_{S_N2}(T)$, i.e.

$$k_{S_N2}(T) = \int_0^{\infty} k_{S_N2}(E_{rel},T)\, P(E_{rel},T)\, dE_{rel} \quad (17)$$

The integration over E_{rel} was carried out numerically by 10-point Gauss−Laguerre quadrature.

Canonical transition state theory is also used to calculate the S_N2 rate constant;[29] i.e.

$$k_{S_N2}(T) = \frac{k_B T}{h} \frac{Q^{\ddagger}_{bar}(T) e^{-E_0/k_B T}}{Q_{rel}(T) Q_{vr}(T)} = \frac{k_B T}{h} e^{-\Delta G^{\ddagger}/k_B T} \quad (18)$$

where $Q^{\ddagger}_{bar}(E,J)$ is the transition state partition function for the central barrier, $Q_{rel}(T)$ is the reactants' relative translation partition function, $Q_{vr}(T)$ is the CH_3Br vibration/rotation partition function, E_0 is the potential difference between the transition state and reactants, and $\Delta G^{\ddagger}$ is the free energy difference between the transition state and reactants.

For the final model, based on microcanonical variational transition state theory (μCVTST), $k_{S_N2}(T)$ is given by[18]

$$k_{S_N2}(T) = \int_0^{\infty} dE \sum_{J=0}^{J_{max}} \frac{k_{cap}(E,J) k_{isom}(E,J)}{k_{dis}(E,J) + k_{isom}(E,J)} P(E,J) \quad (19)$$

$P(E,J)$ is the Boltzmann probability distribution at temperature T for reactants with energy E and rotational angular momentum J, which is given by

$$P(E,J) = \frac{\rho_{reac}(E,J) \exp(-E/k_B T)}{Q_{rel}(T) Q_{vr}(T)} \quad (20)$$

where $\rho_{reac}(E,J)$ is the density of states for the reactants.

The microcanonical rate constants $k_{cap}(E,J)$, $k_{isom}(E,J)$, $k_{dis}(E,J)$ in eq 19 are given by eq 15. For $k_{cap}(E,J)$ the density of states $\rho(E,J)$ is $\rho_{reac}(E,J)$. Thus, inserting the appropriate

(27) Robinson, P. J.; Holbrook, K. A. *Unimolecular Reactions;* Wiley-Interscience: New York, 1972.

(28) Beyer, T.; Swinehart, D. F. *Commun. Assoc. Comput. Machin.* **1973**, *16*, 372.

(29) Canonical variational and conventional TST give the same rate constants for reaction 2; see Truhlar and co-workers, ref 17.

(30) (a) Zhu, L.; Hase, W. L. *Chem. Phys. Lett.* **1990**, *175*, 117. (b) Aubanel, E. E.; Wardlaw, D. M.; Zhu, L.; Hase, W. L. *Int. Rev. Phys. Chem.* **1991**, *10*, 249. (c) Zhu, L.; Chen, W.; Hase, W. L.; Kaiser, E. W. *J. Phys. Chem.* **1993**, *97*, 311.

microcanonical rate constant expressions into eq 19 and canceling common terms yields the simplified expression

$$k_{S_N2}(T) = \frac{1}{hQ_{rel}(T)Q_{vr}(T)} \int_0^\infty dE \sum_{J=0}^{J_{max}} \frac{N^{\ddagger}_{var}(E,J)N^{\ddagger}_{bar}(E,J)}{N^{\ddagger}_{var}(E,J) + N^{\ddagger}_{bar}(E,J)} \exp(-E/k_BT) \quad (21)$$

where $N^{\ddagger}_{var}$ and $N^{\ddagger}_{bar}$ are, respectively, the sums of states for the variational transition state for $Cl^- + CH_3Br$ association and the transition state at the central barrier. As a result of microscopic reversibility, the $Cl^- + CH_3Br \leftrightarrow Cl^-\cdots CH_3Br$ association and dissociation steps have the same variational transition state for a specific E and J. The reaction path for reaction 2 has the rotational symmetry of a symmetric top. Thus, the rotational energy for each transition state is given by

$$E_r(J,K) = \frac{J(J+1)\hbar^2}{2I_a} + \frac{K^2\hbar^2}{2}\left[\frac{1}{I_c} - \frac{1}{I_a}\right] \quad (22)$$

The treatment of the quantum number K has received extensive discussion.[30] For the calculations reported here K is treated as active, so that the transition state sums of states are expressed as[31]

$$N^{\ddagger}_{var}(E,J) = \sum_{K=-J}^{J} (2J+1)N^{\ddagger}_{var}[E - E_{0,var} - E^{\ddagger}_{var}(J,K)] \quad (23)$$

$$N^{\ddagger}_{bar}(E,J) = \sum_{K=-J}^{J} (2J+1)N^{\ddagger}_{bar}[E - E_{0,bar} - E^{\ddagger}_{r,bar}(J,K)] \quad (24)$$

where $E_{0,var}$ and $E_{0,bar}$ represent the potential energy of the variational and the central barrier transition states, respectively. The former depends on E and J. The rotational energies for the two transition states are determined from eq 22 by inserting the correct principal moments of inertia.

Reaction path data of the analytic potential function PES1-(Br) were used to determine the variational transition states for $Cl^- + CH_3Br \leftrightarrow Cl^-\cdots CH_3Br$. The dominant contributor to properties of these transition states is the experimental long-range ion-dipole/ion-induced dipole potential, eq 5, which was accurately fit in deriving PES1(Br). The general chemical dynamics program VENUS[32] was used to obtain the reaction path from PES1(Br) by following the path of steepest decent in mass-weighted Cartesian coordinates with a fourth-order Runga–Kutta numerical integrator. An integration step size of 2×10^{-5} Å·amu$^{1/2}$ was used to give a very accurate path. The projected force constant matrix[33] was formed and diagonalized, during this numerical integration, to obtain the frequencies along the reaction path. The only vibrational frequency that undergoes a significant change along the reaction path is that for the degenerate $Cl^-\cdots C-Br$ bending mode. Its value is plotted in Figure 1 as a function of the $Cl^-\cdots C$ distance.

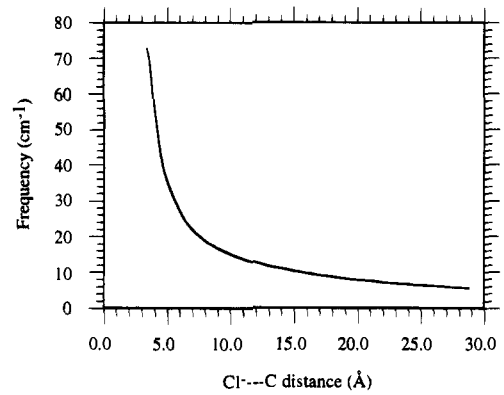

Figure 1. The $Cl^-\cdots C-Br$ degerate bending frequency as a function of $Cl^-\cdots C$ distance.

The variational sum of states in eq 21 is determined by minimizing the sum of states as a function of the reaction path. As for the above capture/RRKM model, Beyer–Swinehart direct counting[28] was used to calculate the sum of states. These resulting variational sums of states versus E and J were then inserted into eq 21, and the integration over E was done numerically, by 10-point Gauss–Laguerre quadrature. To within three significant figures this integration gave the same result as 40-point Gauss–Laguerre quadrature. The upper limit for the summation over J in eq 21 was set to $J_{max}(E)$, which was determined by setting $K = 0$ in eq 22 and solving for J versus E.

The two limiting cases for eq 21 occur when $N^{\ddagger}_{var} \gg N^{\ddagger}_{bar}$ and $N^{\ddagger}_{bar} \gg N^{\ddagger}_{var}$ for all E and J. Though neither of these limits are attained for reaction 2, it is of interest to consider the form of $k_{S_N2}(T)$ for these limits. With $N^{\ddagger}_{var} \gg N^{\ddagger}_{bar}$ at all E and J and the potential energy of the central barrier higher than that of the reactants [not the case for reaction 2], eq 21 becomes

$$k_{S_N2}(T) = \frac{e^{-E_{0,bar}/k_BT}}{hQ_{rel}(T)Q_{vr}(T)} \int_0^\infty dE^{\ddagger} \sum_{J=0}^{J_{max}} N^{\ddagger}_{bar}(E^{\ddagger},J) \exp(-E^{\ddagger}/k_BT) \quad (25)$$

where $E = E^{\ddagger} + E_{0,bar}$. The lower limit of the integral in eq 25 can be set to zero instead of $-E_{0,bar}$, since $N^{\ddagger}_{bar}(E^{\ddagger},J)$ is zero for $E^{\ddagger}$ less than zero. The partition function for the central barrier transition state can be written as the Laplace transform of the sum of states at the central barrier,[34] so that

$$Q^{\ddagger}_{bar}(T) = \frac{1}{k_BT} \int_0^\infty dE^{\ddagger} \sum_{J=0}^{J_{max}} (2J+1)N^{\ddagger}_{bar}(E^{\ddagger},J) \exp(-E^{\ddagger}/k_BT) \quad (26)$$

Thus, eq 25 simply becomes the TST rate constant in eq 18.

For $N^{\ddagger}_{bar} \gg N^{\ddagger}_{var}$ at all E and J, the S_N2 rate constant becomes the μCVTST rate constant for ion–molecule capture. The expression for $k_{S_N2}(T)$ is

$$k_{S_N2}(T) = \frac{1}{hQ_{rel}(T)Q_{vr}(T)} \int_0^\infty dE \sum_{J=0}^{J_{max}} N^{\ddagger}_{var}(E,J) \exp(-E/k_BT) \quad (27)$$

Since $N^{\ddagger}_{var}$ is chosen variationally and the transition state structure varies with E and J, the integral in eq 27 can not be

(31) In previous work (i.e., ref 30) the term $(2J + 1)$ has not been included in the expression for the sum of states. This can be done when calculating $k(E,J)$, eq 15, since the $(2J + 1)$ term appears in both the sum and density of states and, thus, cancels.

(32) Hase, W. L.; Duchovic, R. J.; Hu, X.; Lim, K. F.; Lu, D.-h.; Peslherbe, G. H.; Swamy, K. N.; Vande Linde, S. R.; Wang, H.; Wolf, R. J. VENUS, to be submitted to the Quantum Chemistry Program Exchange. VENUS is an enhanced version of MERCURY, Hase, W. L. QCPE **1983**, *3*, 453.

(33) Miller, W. H.; Handy, N. C.; Adams, J. E. *J. Chem. Phys.* **1980**, *72*, 99.

(34) Forst, W. *Theory of Unimolecular Reactions;* Academic Press: New York, 1973.

Table 3. Thermal Rate Constants for $Cl^- + CH_3Br \rightarrow ClCH_3 + Br^-$ Substitution[a]

		conventional TST[b]								
			ab initio[e]		PES1(Br)[f]		μCVTST/PES1(Br)[g]		eq 17/PES1(Br)[h]	
T (K)	exp[c]	AM1/SRP[d]	har	anhar	har	anhar	har	anhar	har	anhar
207	1.9	3.1	2.7 (2.4)	2.5 (2.2)	2.2	2.0	1.8	1.7	1.7	1.7
300	1.4	1.4	1.4 (1.4)	1.4 (1.4)	1.4	1.4	1.4	1.4	1.4	1.4
538	0.84	0.96	1.2 (1.3)	1.3 (1.5)	1.4	1.5	1.5	1.5	1.7	1.7
564	0.90	0.96	1.2 (1.4)	1.3 (1.6)	1.5	1.6	1.6	1.5	1.8	1.7
fitted E_b[i]		−1.51	-1.16 (-1.11)	-1.09 (-1.01)	−1.33	−1.39	−1.44	−1.59	−1.53	−1.71
fitted $E_{0,bar}$[j]		−1.54	-1.35 (-1.25)	-1.28 (-1.13)	−1.17	−1.07	−1.28	−1.27	−1.37	−1.39

[a] Rate constants are in units of 10^{10} L mol^{-1} s^{-1}. [b] The conventional TST rate constants are calculated using eq 18. [c] Experimental rate constants by Viggiano and co-workers, ref 17. [d] AM1/SRP potential with adjusted parameters; Truhlar and co-workers, ref 17. [e] MP2/SV4PP/6-31G* and HF/SV4PP/6-31G* potentials. Rate constants for the latter are given in parentheses. [f] Analytic empirical potential energy surface PES1(Br). [g] The μCVTST rate constants were calculated using eq 21 and PES1(Br). [h] This rate constant was calculated using the capture/RRKM model of eq 17 and PES1(Br). [i] E_b is the classical potential difference between the barrier and reactants required to fit the 300 K experimental rate constant. [j] Zero-point energy difference between the transition state of the central barrier and the reactants. Determined from the fitted E_b and the harmonic (or harmonic) frequencies.

related to a partition function as is done in eqs 25 and 26. Thus, eq 27 must be solved numerically. For $Cl^- + CH_3Br$ capture, eq 27 gives a rate constant nearly identical to those of the trajectory capture and the statistical adiabatic channel models.[15]

The potential energy of the $Cl^- + CH_3Br$ central barrier is less than that of the reactants so that for any temperature there will always be some E and J for which $N^{\ddagger}_{bar} > N^{\ddagger}_{var}$. However, for higher temperatures, these E and J begin to make a smaller contribution to the rate constant and it may become accurate to assume $N^{\ddagger}_{bar} < N^{\ddagger}_{var}$. Then $k_{S_N2}(T)$ can be written as in eq 25, where $E_{0,bar}$ is the negative potential energy difference between the central barrier and reactants. However, now the lower limit to the integral, $-E_{0,bar}$, is a positive number and the μCVTST and TST $k_{S_N2}(T)$ are not equivalent; i.e. in μCVTST the minimum energy of the transition state is $-E_{0,bar}$, while in TST it is zero. The μCVTST expression for $k_{S_N2}(T)$ is

$$k_{S_N2}(T) = \frac{k_B T(Q^{\ddagger}_{bar} - \chi)}{hQ_{rel}(T)Q_{vr}(T)} \exp(-E_{0,bar}/k_B T) \qquad (28)$$

where χ is given by

$$\chi = \frac{1}{k_B T}\int_0^{-E_{0,bar}} dE^{\ddagger} \sum_{J=0}^{J_{max}} (2J+1)N^{\ddagger}_{bar} \exp(-E^{\ddagger}/k_B T) \qquad (29)$$

When the potential of the central barrier is higher than that of the reactants, $-E_{0,bar}$ is negative and χ is zero. However, for a S_N2 reaction like $Cl^- + CH_3Br$ the central barrier lies below the reactants. Then $-E_{0,bar}$ is positive and $\chi > 0$. As a result the μCVTST S_N2 rate constant is smaller than the TST value. Whether one can neglect χ and equate the μCVTST and TST rate constants depends on the value of $E_{0,bar}$ and the temperature considered. In the next section, the conventional TST, eq 18, and the μCVTST, eq 21, expressions for the $Cl^- + CH_3Br \rightarrow ClCH_3 + Br^-$ rate constants are compared.

It is helpful to estimate at what value of $E^{\ddagger}$ the term $N^{\ddagger}_{var} \exp(-E^{\ddagger}/k_B T)$ in eq 29 reaches the maximum if $E_{0,bar}$ is negative. For this purpose we use the Whitten–Rabinovitch approximation[27] for $N^{\ddagger}_{bar}$; i.e.

$$N^{\ddagger}_{bar} = \frac{(E^{\ddagger} + aE_z^{\ddagger})}{s!\prod_{i=1}^{s} h\nu_i} \qquad (30)$$

where s is the number of vibrational modes at the transition state, $E_z^{\ddagger}$ is the zero-point energy of the central barrier, and a is a parameter that has the limits of 0 and 1 for $E^{\ddagger} \rightarrow 0$ and $E^{\ddagger} \rightarrow \infty$. For this analysis the original approximation of Rabinovitch and Diesen,[35] that $da/dE^{\ddagger}$ is negligibly small, was used, so that taking the derivative of $N^{\ddagger}_{var} \exp(-E^{\ddagger}/k_B T)$ with respect to $E^{\ddagger}$ and setting it be zero gives

$$(E^{\ddagger})^* = sk_B T - aE_z^{\ddagger} \qquad (31)$$

$(E^{\ddagger})^*$ is the energy at which $N^{\ddagger}_{bar} \exp(-E^{\ddagger}/k_B T)$ reaches a maximum. If this value is between 0 and $-E_{0,bar}$ or close to this range, the integrated value of eq 29, χ, cannot be neglected compared with $Q^{\ddagger}_{bar}$. In this case, the μCVTST rate constant will obviously deviate from that of conventional TST. By estimating the value of $(E^{\ddagger})^*$ and comparing that with the value of $-E_{0,bar}$, one can roughly tell whether the difference between μCVTST and conventional TST is large or not. Also, from eq 31, it is seen that $sk_B T$ is an upper bound for $(E^{\ddagger})^*$ and can be used for estimation purposes.

The following conclusions can be drawn from eq 31. First, at low temperature $sk_B T$ can be within the same order of magnitude or smaller than $-E_{0,bar}$, meaning the maximum of the term $N^{\ddagger}_{bar} \exp(-E^{\ddagger}/k_B T)$ lies within or close to the integration range of eq 29 and therefore χ cannot be neglected in eq 28. Second, if the number of vibrational modes is small, $sk_B T$ can be the same order of magnitude as $-E_{0,bar}$. One cannot neglect χ in this case, even for a moderate value of $-E_{0,bar}$ (e.g., 1 kcal/mol). Third, if $-E_{0,bar}$ is a very large number, χ cannot be neglected in the rate constant expression.

For reaction 2 there are 11 modes at the transition state. For the temperature range used in the rate constant calculations reported here, both $sk_B T$ and $(sk_B T - aE_z^{\ddagger})$ are within the same order of magnitude as $-E_{0,bar}$. This means χ cannot be neglected. Therefore some differences are expected between the microcanonical and canonical transition state theory calculations on the same potential surface. This fact is reflected by the adjusted central barrier height values presented in the next section.

IV. $Cl^- + CH_3Br \rightarrow ClCH_3 + Br^-$ Rate Constant

A. Rate Constant Versus Temperature. Rate constants for reaction 2 have been determined in the low-pressure limit by Viggiano and co-workers[17] and their measured values are listed in Table 3. Truhlar and co-workers[17] have used conventional TST[29] to calculate the rate constant for reaction 2 and compare with the experimental measurements. They used an

(35) Rabinovitch, B. S.; Diesen, R. W. *J. Chem. Phys.* **1959**, *30*, 735.

Table 4. k_H/k_D Kinetic Isotope Effect for $Cl^- + CH_3Br \rightarrow ClCH_3 + Br^-$ [a]

		conventional TST								
			ab initio		PES1(Br)		μCVTST/PES1(Br)		eq 17/PES1(Br)	
T(K)	exp	AM1/SRP	har	anhar	har	anhar	har	anhar	har	anhar
207	0.81 ± 0.03	0.88	0.96 (0.72)	0.98 (0.73)	0.60	0.53	0.76	0.60	0.70	0.55
300	0.81 ± 0.03	0.93	0.99 (0.75)	1.00 (0.75)	0.72	0.68	0.79	0.64	0.76	0.60
538	0.89 ± 0.06	0.97	0.96 (0.76)	0.99 (0.76)	0.84	0.85	0.86	0.89	0.90	0.73
564		0.97	0.96 (0.76)	0.99 (0.76)	0.85	0.86	0.87	0.93	0.91	0.74

[a] The different statistical theory calculations are described in the footnotes to Table 3.

AM1 potential energy surface, with the atomic core elements of the AM1 semiempirical theory adjusted to match the experimental heat of reaction and the 300 K rate constant. Their rate constants, calculated using harmonic frequencies, are listed in Table 3. Qualitative agreement with the experimental rate constants was obtained. However, the lowest temperature rate constant at 207 K was overestimated by >50%. Their adjusted AM1 surface had a classical potential energy difference between the central barrier and reactants of −1.51 kcal/mol.

In this work, we have calculated the rate constant for reaction 2 using conventional TST and PES1(Br), with vibrational frequencies treated as harmonic. As done in the above work of Truhlar and co-workers,[17] the classical potential energy barrier of PES1(Br) was adjusted to match the 300 K experimental rate constant. The adjusted value for the barrier is −1.33 kcal/mol. The rate constants determined from these calculations are listed in Table 3. Good agreement with experiment is obtained at 207 K. However, at 538 and 564 K, the calculated rate constants are ~50% too large.

Additional statistical theory calculations of the rate constant for reaction 2 are also presented here. Conventional TST calculations are given for PES1(Br) with anharmonic frequencies, and for the HF and MP2 *ab initio* surfaces with both harmonic and anharmonic frequencies. PES1(Br) is also used in μCVTST calculations, eq 21, and in a calculation employing the capture/RRKM model, eq 17. Both harmonic and anharmonic frequencies are used for these two calculations. The results of these additional statistical theory calculations are presented in Table 3. For each of these calculations, the classical potential energy difference between the central barrier and reactants was adjusted to fit the experimental rate constant at 300 K.

The results in Table 3 show that anharmonicity has a negligible effect on the temperature dependence of the rate constants. The μCVTST and the conventional TST rate constants for PES1(Br) are similar, with the μCVTST values showing a slightly less negative temperature dependence. The fitted E_b is more negative for the μCVTST calculations than for the conventional TST calculations. This is because, at the same value of E_b, μCVTST gives a smaller rate constant than does the conventional TST; see Eqs 28−31. A comparison of the results of the μCVTST and capture/RRKM calculations in Table 3 shows that these two theoretical models give nearly the same temperature dependent rate constants and fitted E_b values. The phase space theory calculation by Graul and Bowers,[1] of the $Cl^- + CH_3Br$ rate, is similar to these μCVTST and capture/RRKM calculations and gives a similar temperature dependent rate constant.

In summarizing the results in Table 3, not one of the different statistical models and potential energy surfaces gives a quantitative fit to the experimental rate constants. The fitted values for E_b vary from −1.01 to −1.71 kcal/mol. The temperature dependence of the rate constant is dominated by the exponential term $\exp(-E_{0,bar}/k_bT)$ in Eqs 18 and 28. From the $E_{0,bar}$ values in Table 3 the AM1/SRP calculations is expected to have the most negative temperature dependence and this is indeed the case.

B. k_H/k_D Kinetic Isotope Effect. The different statistical models and potential energy surfaces used to calculate the rate constant for reaction 2 versus temperature are also used to calculate the k_H/k_D kinetic isotope effect for reaction 2. The results are given in Table 4, where they are compared with the experimental results and the previous AM1/SRP calculations of Truhlar and co-workers.[17] The E_b values, given in Table 3 and which give a fit to the experimental k_H rate constant for reaction 2 at 300 K, were used in the calculations of k_H/k_D reported here.

The results in Table 4 show that the calculations performed at the harmonic level give better agreement with the experimental k_H/k_D ratios than do the anharmonic calculations. The μCVTST calculations carried out at the harmonic level, with the PES1(Br) analytic potential, are in the best agreement with the experimental results. The TST calculation, based on the harmonic frequencies of the AM1/SRP potential, also gives good agreement with experiment. Strikingly, the use of anharmonic frequencies reduces the agreement between the calculations and experiment. This is somewhat bothersome, since it is generally thought that anharmonic frequencies more accurately represent the vibrational properties of the potential energy surface than do harmonic frequencies.

C. Rate Constant versus E_{rel} and CH_3Br Temperature. The statistical theory expression in eq 16 was used to calculate the rate constant for reaction 2 versus $Cl^- + CH_3Br$ relative translational energy E_{rel} and the CH_3Br temperature. The calculations were performed with PES1(Br) and the value used for E_b is that given above which gives a fit to the thermal rate constant at 300 K when using eq 17. This latter equation results when eq 16 is integrated over the Boltzmann distribution for E_{rel}. It is of interest to determine whether the same theoretical model and potential energy surface can fit both the thermal rate constants for reaction 2 and the rate constants versus fixed E_{rel}.

The rate constant for reaction 2 was calculated at fixed E_{rel} in the range of 0.5 to 2.5 kcal/mol and for CH_3Br temperatures of 207, 300, 538, and 564 K. These energy and temperature ranges are the same as those for the experiments.[2] The calculated and experimental results are compared in Figure 2. The calculated values are the same order of magnitude as the experimental ones by Viggiano and co-workers.[2] Also, the general trend of the calculated rate constant versus relative translational energy is the same as that observed in the experiment; i.e., the rate constant decreases with an increase in relative translational energy. However, the decrease in the calculated rate constant, with an increase in E_{rel}, is much less than that observed in the experiments. In addition, at higher E_{rel} the calculated rate constant becomes nearly constant, while the experimental ones continue to decrease. A striking difference between the calculated and experimental rate constants is the effect of CH_3Br temperature. As the CH_3Br temperature

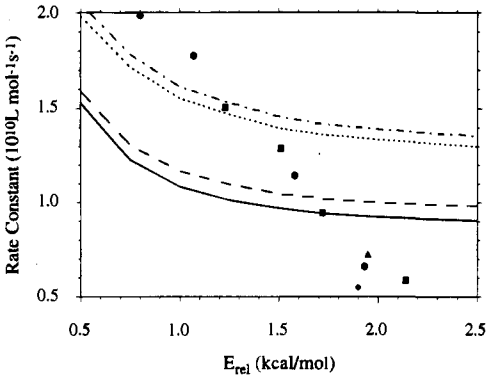

Figure 2. Rate constant versus $Cl^- + CH_3Br$ relative translational energy and CH_3Br temperature. The curves are calculated values: (—) 207 K, (— —) 300 K, (- - -) 538 K, and (— - —) 564 K. The points—(●) 207 K, (■) 300 K, (◆) 538 K, and (▲) 564 K—are experimental values from ref 2.

increases, the calculated rate constant increases if E_{rel} is kept constant. This is in contrast with the experimental observation that the rate constant is nearly independent of CH_3Br temperature changes. Combined with previous theoretical and experimental work,[1-14] the disagreement found here between the calculated and experimental $k(E_{rel},T)$ suggests non-statistical behavior for reaction 2.

It is worth noting that in our preliminary calculations of $k(E_{rel},T)$ in eq 16, the WR approximation[27] was used to calculate the sums of states for the transition states. However, this approximation was rejected because it over-counted the sum of states, particularly for small vibrational energies in the transition state, when the W-R sum of states was 2−4 times larger than that of the BS direct count.[28] As a result of the large total angular momentum J for the $Cl^- + CH_3Br$ reaction, which makes the transition state rotational energy large, small transition state vibrational energies are important in evaluating eq 16. The effect of using the WR approximation was to make $k(E_{rel},T)$ nearly independent of T, as found in the experiment. This erroneous result, based on the WR approximation, illustrates the sensitivity of the calculated $k(E_{rel},T)$ to specific details of the calculational procedure.

The increase in $k(E_{rel},T)$ with an increase in T may seem surprising, since the potential energy of the central barrier is lower than that of the reactants. However, $Cl^- + CH_3Br$ collisions form complexes with an angular momentum which gives rise to a large centrifugal potential energy at the central barrier. The l_{max} values (see Section IIIA) for E_{rel} of 0.5, 1.0, and 2.0 kcal/mol give a centrifugal potential at the central barrier of 3.9, 5.1, and 6.7 kcal/mol, respectively. Thus, the total potential energy at the central barrier is higher than the potential energy of the reactants for large impact parameter collisions and a positive temperature dependent rate is not surprising.

The calculation of $k(E_{rel},T)$ performed here involves a lengthy multidimensional integration. Since the reactant orbital angular momentum is large and may be dominant in forming the total angular momentum J, two approximate calculations were performed in which the integrations over j and j_z in eq 16 were removed. In one calculation the CH_3Br rotational energy was removed from eq 14 and for the other the CH_3Br rotational energy was fixed at $^3/_2\ RT$. The same E_b was used for these two calculations as that used above for the complete integration over j and j_z. The results of these approximate calculations and the complete integration are compared in Table 5, for the lowest and highest temperatures considered here. The rate constants for the approximate calculation, with $E_{rot} = {}^3/_2RT$, are nearly the same as those for the complete integration. The approximate calculation, with $E_{rot} = 0$, gives rate constants too large at low E_{rel} and too small at high E_{rel}. Neither one of the two approximate calculations gives a near temperature independent rate constant as found from experiment.[2]

Table 5. Effect of Different Treatments of the CH_3Br Rotational Angular Momentum on $k(E_{rel},T)$[a]

	T = 207 K			T = 564 K		
E_{rel}	j,j_z[b]	$E_{rot} = {}^3/_2RT$[c]	$E_{rot} = 0$[d]	j,j_z[b]	$E_{rot} = {}^3/_2RT$[c]	$E_{rot} = 0$[d]
0.50	1.53	1.56	2.02	2.05	1.99	2.44
0.75	1.23	1.27	1.35	1.78	1.78	1.88
1.00	1.08	1.14	1.10	1.61	1.67	1.63
1.25	1.01	1.05	0.99	1.53	1.61	1.50
1.50	0.97	1.01	0.93	1.46	1.55	1.40
1.75	0.94	0.97	0.88	1.41	1.52	1.34
2.00	0.92	0.96	0.86	1.39	1.48	1.30
2.50	0.90	0.93	0.84	1.35	1.45	1.25

[a] The rate constant is in units of 10^{10} L mol^{-1} s^{-1}. E_{rel} is in units of kcal/mol. [b] Integration over j and j_z as given by eq 16. These results are plotted in Figure 2. [c] Integration over j and j_z removed from eq 16. The rotational energy in eq 14 is set to $^3/_2\ RT$. [d] Integration over j and j_z removed from eq 16. The rotational energy in eq 14 is set to zero.

V. Summary

In the work presented here three different potential energy surfaces, with both harmonic and anharmonic frequencies, and three different statistical models are used to calculate the rate constant for the $Cl^- + CH_3Br \rightarrow ClCH_3 + Br^-$ S_N2 reaction versus temperature, the k_H/k_D isotope effect for this reaction, and the reaction rate constant versus $Cl^- + CH_3Br$ relative translational energy E_{rel} and CH_3Br temperature. When applying one of the theoretical models, the classical potential energy barrier E_b for each potential energy surface was adjusted to fit the 300 K experimental k_H thermal rate constant. The three statistical models considered here are conventional TST [eq 18], μCVTST with both dissociation and isomerization of the Cl^-- - -CH_3Br complex treated [eq 21], and an ion-molecule capture/RRKM model which also accounts for dissociation and isomerization of the complex [eqs 16 and 17]. The following are the important findings of this study:

1. The general trend of the experimental rate constant versus temperature can be reproduced, but a quantitative fit is not obtained. Using anharmonic instead of harmonic frequencies affects the fitted E_b values, but has a negligible effect on the rate constant's temperature dependence. For the conventional TST calculations the fitted value of E_b varies by 0.5 kcal/mol, depending on which potential energy surface is used. Using the same potential energy surface but varying the theoretical method gives fitted values of E_b which vary by 0.3 kcal/mol. If the same potential energy surface and E_b value are used, μCVTST gives a smaller rate constant than does conventional TST. Therefore, to fit the experimental rate constants a smaller E_b is required for the μCVTST calculation.

It might be possible to use an unusual set of vibrational frequencies for the central barrier transition state to fit the experimental temperature dependent S_N2 rate constant with a statistical rate theory. However, three different potential energy surfaces with both harmonic and anharmonic frequencies were used in this work and Graul and Bowers[1] used a different potential with harmonic frequencies in their calculation. Thus, seven different potential energy surfaces have been considered and not one, when used with a statistical theory, gives a temperature dependent rate that matches the experiment.

2. The calculated k_H/k_D kinetic isotope effect is very sensitive to whether harmonic or anharmonic frequencies are used in the calculations. The values used for E_b to calculate k_H/k_D are those

which fit the experimental rate constant for $Cl^- + CH_3Br \rightarrow ClCH_3 + Br^-$ at 300 K. The previous TST calculations of Truhlar and co-workers[17] with the AM1/SRP potential and the current μCVTST/PES1(Br) calculation, both with harmonic frequencies, give the best fit to the experimental k_H/k_D ratios, with the latter the better of the two. However, it is worrisome that the harmonic frequencies give k_H/k_D ratios which tend to agree with experiment, while the anharmonic frequencies do not, since the latter are generally thought to more accurately represent the actual vibrational motions.

3. Using PES1(Br) and the value of E_b which gives a fit to the 300 K experimental $Cl^- + CH_3Br$ S_N2 rate constant, the rate constant was also calculated versus E_{rel} and CH_3Br temperature. Though the calculated and experimental[2] rate constants are within the same range, they have qualitative differences. The decrease in the calculated rate constant with an increase in E_{rel} is more gradual and less sharp than for the experimental rate constant. Also the calculated rate constant increased with CH_3Br temperature T, while the experimental rate constant is nearly independent of T. In an extension of the ADO/RRKM calculations of ref 1b, Graul[36] finds that $k(E_{rel},T)$ varies with T in a manner similar to that found here.

The work reported here indicates that statistical rate theories can reproduce some aspects of the experimental rate constants for reaction 2, but cannot in a self-consistent way reproduce the dependence of the experimental rate constant on temperature, isotope substitution, and reagent relative translational energy and internal temperature. There also is substantial uncertainty in the qualitative agreement reached with certain aspects of the experimental measurements, since the potential energy of the central barrier was treated as an adjustable parameter and it is not known whether the resulting fitted barrier height is accurate. The rate constants calculated here are for the low-pressure limit. In a previous harmonic TST analysis using PES1(Br),[15] it was found that a classical central barrier of −2.0 kcal/mol is needed to fit the high-pressure rate constant for reaction 2. This fitted PES1(Br) barrier is 0.7 kcal/mol lower than that required here to fit the low-pressure experimental rate constant with PES1(Br) and harmonic TST.

The inability of statistical theories to adequately interpret the experimental kinetics for reaction 2 is consistent with previous trajectory calculations,[6-12] which indicate non-statistical properties for both reaction 2 and the $Cl^- + CH_3Cl$ S_N2 reaction. Weak coupling and slow energy transfer between the CH_3Br intramolecular modes of the Cl^-- - -CH_3Br complex are predicted from the trajectories. As a result the following dynamical attributes are expected for the $Cl^- + CH_3Br$ S_N2 reaction: (1) the $Cl^- + CH_3Br \rightarrow Cl^-$- - -$CH_3Br$ association rate constant is smaller than that predicted by μCVTST and the trajectory capture model; (2) the dissociation and isomerization kinetics of the Cl^-- - -CH_3Br complex are non-RRKM; and (3) recrossings of the [Cl- - -CH_3- - -Br]$^-$ central barrier are important. We are currently trying to formulate an expression for the $Cl^- + CH_3Br$ S_N2 rate constant which will incorporate these dynamical attributes.

Acknowledgment. This research was supported by the National Science Foundation.

JA951398F

(36) Graul, S. Private communication.